JOURNAL OF PHYSICAL ORGANIC CHEMISTRY
J. Phys. Org. Chem. 2005; **18:** 962–973
Published online 19 April 2005 in Wiley InterScience (www.interscience.wiley.com). DOI: 10.1002/poc.935

Experimental and theoretical studies of 2,5-diphenyl-1,4-distyrylbenzenes with all-*cis*- and all-*trans* double bonds: chemical structure determination and optical properties

Zengqi Xie,[1] Bing Yang,[1] Linlin Liu,[1] Mao Li,[1] Dong Lin,[1] Yuguang Ma,[1]* Gang Cheng[2] and Shiyong Liu[2]

[1]Key Laboratory for Supramolecular Structure and Materials of the Ministry of Education, Jilin University, 130012 Changchun, China
[2]National Laboratory of Integrated Optoelectronics, Jilin University, 130023 Changchun, China

Received 20 August 2004; revised 22 October 2004; accepted 18 February 2005

ABSTRACT: 2,5-Diphenyl-1,4-distyrylbenzene (DPDSB) with all-*cis* (*cis*-DPDSB) and all-*trans* double bonds (*trans*-DPDSB) were synthesized by Wittig reaction and the differences in structural and optical properties between the *cis*- and *trans*-isomers are discussed in detail. Both compounds were fully characterized by NMR spectroscopy, FT-IR spectroscopy, x-ray crystallography, differential scanning calorimetry (DSC) and electrochemical methods. X-ray analysis and molecular simulation revealed that the structure of *cis*-DPDSB obviously deviates from planarity along both the distyrylbenzene and terphenyl directions, and less intermolecular interaction exists in crystal. The *cis*-isomer shows a large blue shift in the absorption spectrum in comparison with that of the *trans*-isomer, and cyclic voltammetric measurements give bandgaps of 3.16 and 2.97 eV for *cis*- and *trans*-DPDSB, respectively. Both compounds show unusually strong blue fluorescence in the solid state, probably due to the weak intermolecular interaction existing in both isomers owing to the large steric hindrance induced by the substituted phenyl groups. DSC experiments determined that both isomers have excellent thermal stability, which indicates that they can be used as active layers to make stable devices. Quantum chemical calculations for the frontier molecular orbital and the cation and anion properties reveal that the HOMO and LUMO are completely localized in the distyrylbenzene direction and the distyrylbenzene segment has more sensitive electroactivity than the terphenyl segment whether it is *cis*- or *trans*-DPDSB. Copyright © 2005 John Wiley & Sons, Ltd.

KEYWORDS: *cis*/*trans* isomers; 2,5-diphenyl-1,4-distyrylbenzene; luminescence; oligomeric phenylenvinylene; theoretical calculation; Wittig reactions

INTRODUCTION

Conjugated polymers are key components of a number of advanced but fairly in expensive electronic devices.[1–4] Some of the most promising candidates for the active layer in organic light-emitting diodes (LEDs) are polymers derived from poly(*p*-phenylenevinylene) (PPV), such as MEH-PPV,[5,6] DP-PPV[7–9] and CN-PPV.[10,11] The concept behind the molecular design of such PPVs is the use of substitutional side-chains to improve solubility in common solvents and suppress molecular aggregation.[2] Nevertheless, there still exists a significant tendency towards molecular aggregation for PPVs with, e.g., alkoxy side-chains, which gives rise to strong effects on their light emission properties.[12–18] Almost all PPVs with substituted phenyl (DP-PPV) have very high efficiency since the bulky substitution effectively suppresses the aggregation.[19–21] The oligomers of the repeating unit of a polymer are often useful in understanding the properties of a polymer system.[22–27] This is due to the close analogy of their physical properties, and as easier characterization of the oligomeric system. The oligomers themselves as active materials have been used widely owing to their definite structure.[28–31] Several papers have reported the synthesis of a series of short-chain oligomeric analogues of PPVs with alkoxy groups,[32–34] but to our knowledge, discussion about oligomers corresponding to phenyl-substituted PPVs is limited.[35]

In all kinds of PPVs, the presence of *cis*/*trans*-vinylene units and their photochemical isomerization attracts special attention because the *cis*-isomer generally shows weak luminescence and is regarded as a *cis* defect.[36–39] Although great efforts have been made in the investigation of relationships that exist between the *cis*/*trans* conformation in polymer chains and the resulting luminescence properties, the understanding of these dependences is still incomplete, which is partially due to a lack

**Correspondence to:* Y. Ma, Key Laboratory for Supramolecular Structure and Materials of the Ministry of Education, Jilin University, 2699 Qianjin Avenue, 130012 Changchun, China.
E-mail: ygma@jlu.edu.cn
Contract/grant sponsor: National Science Foundation of China;
Contract/grant numbers: 20474024; 20125421; 90101026; 50303007.
Contract/grant sponsor: Ministry of Science and Technology of China;
Contract/grant numbers: 2002CB6134003; 2003CB314703.

of more definite structural information on polymer systems.[40–42] So far the results on this topic have come mostly from theoretical simulation,[35] and need urgently to be testified by experiment.

In this paper, we report the synthesis and characterization of the most basal model compounds (oligomers) for DP-PPV and discuss the differences between *cis*- and *trans*-isomers in detail. Such ordinary materials themselves exhibit excellent optical and thermal properties, which are useful in making luminescence devices or lasers.

RESULTS AND DISCUSSION

Synthesis of *cis*- and *trans*-DPDSB

The synthetic route toward the target materials is outlined in Scheme 1. *cis*-DPDSB was synthesized by a twofold Wittig reaction from benzyltriphenylphosphonium bromide and 1,1′;4′,1″-terphenyl-2′,5′-dicarbaldehyde (**3**) in tetrahydrofuran (THF) solution by dropping potassium *tert*-butylate (*t*-BuOK, dissolved in THF) over a period of 30 min, and then stirring the mixture for another 12 h at room temperature. Colorless crystals were obtained after the product had been deposited in methanol (yield: 87%). Interestingly, the resulting product is determined to have the all-*cis* conformation as discussed below. Previous studies on the Witting reaction by Hwang *et al.* demonstrated that reaction in the polar solvents produced more *cis* products (*Z*-selectivity).[43] They also indicate using *ortho*-substituted benzaldehydes bearing electron-withdrawing substituent such as CF_3 exhibit a pronounced enhancement for *Z*-selectivity (*Z*/*E* ratio up to 5.6). Our results indicate that pure *cis*-DPDSB can be obtained directly by the optimized synthetic procedure probably owing to the *o*-phenyl substituent playing the same role as the CF_3 substituent in the Witting reaction. *trans*-DPDSB was prepared by refluxing a *p*-xylene solution of the *cis*-isomer for 12 h, with a small amount of iodine as catalyst (yield: 95%).

Structural determination of *cis*- and *trans*-DPDSB

Based on NMR and FT-IR measurements (Figs 1–3), the two compounds are unambiguously characterized as *cis*- and *trans*-DPDSB, respectively (shown in Scheme 2). The ^1H and ^{13}C NMR spectra are shown in Figs 1 and 2, which are correlated by ^{13}C, ^1H chemical shift correlation spectroscopy, and the chemical shifts are given in Table 1. The position, intensity and coupling patterns of the NMR signals provide unequivocal proof of the structures of the isomers. For example, the chemical shifts of the olefinic

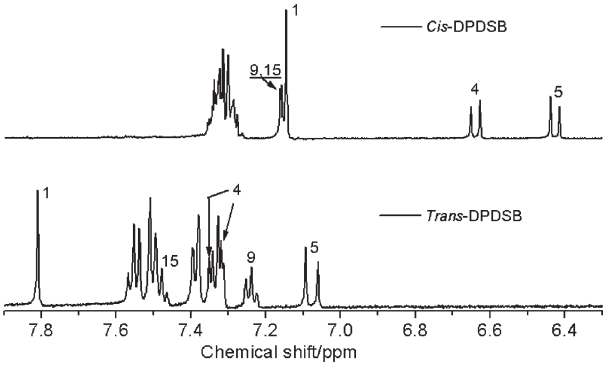

Figure 1. ^1H NMR spectra of *cis*- and *trans*-DPDSB. The numbers correspond to the numbers in Scheme 2

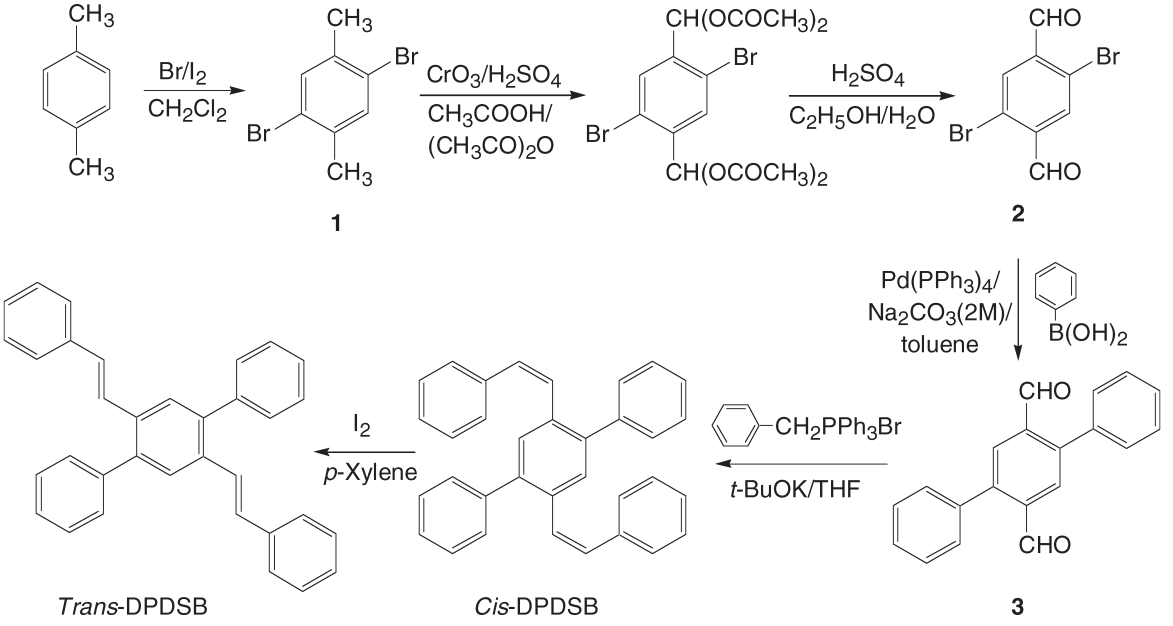

Scheme 1. Synthesis route to *cis*- and *trans*-DPDSB

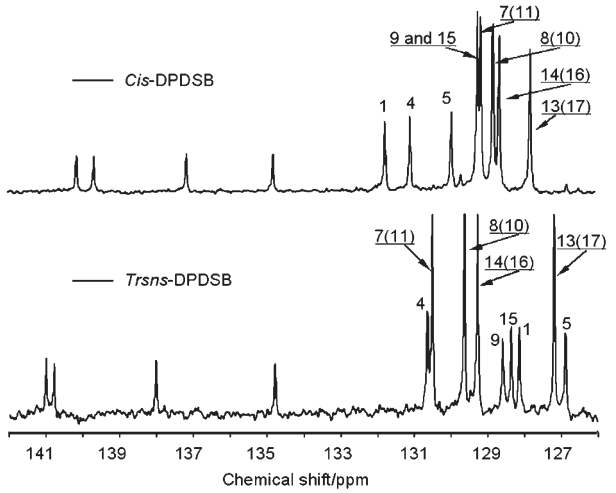

Figure 2. ^{13}C NMR spectra of *cis*- and *trans*-DPDSB. The numbers correspond to the numbers in Scheme 2

protons are 6.4 ppm (H4) and 6.6 ppm (H5) with coupling constant 12 Hz in the *cis* configuration and 7.1 ppm (H4) and 7.3 ppm (H5) with coupling constant 16.3 Hz in the *trans* configuration.[44] The reason for the signals of the olefinic protons in *trans*-DPDSB shifting downfield compared with those in the *cis*-isomer is the decreased shielding effect of the phenyl ring on the olefinic protons and the decreased electron cloud density on the olefinic segments, because *trans*-DPDSB exhibits more planarity and a greater conjugated effect in the distyrylbenzene direction than that of the *cis*-isomer (see the discussion below). The dispersed electron cloud also affects the signals of protons in phenyl rings. By ^{1}H NMR of *trans*-DPDSB, we investigated the clear difference between the protons in end phenyl rings in the distyrylbenzene direction and the terphenyl direction, e.g. $\delta = 7.24$ ppm for H9 and $\delta = 7.48$ ppm for H15. Such a difference arises because of the effective conjugation in the distyrylbenzene direction (planar conformation) and less conjugation in the terphenyl direction (twist conformation) in *trans*-DPDSB. In the ^{1}H NMR spectra of *cis*-DPDSB, the δ values of H9 and H15 are localized in the same range and become indistinguisable, reflecting

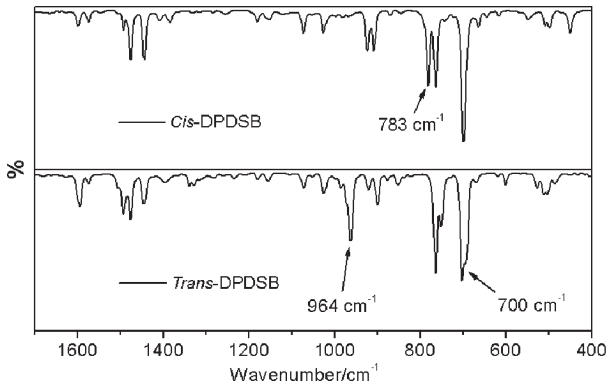

Figure 3. FT-IR spectra of *cis*- and *trans*-DPDSB

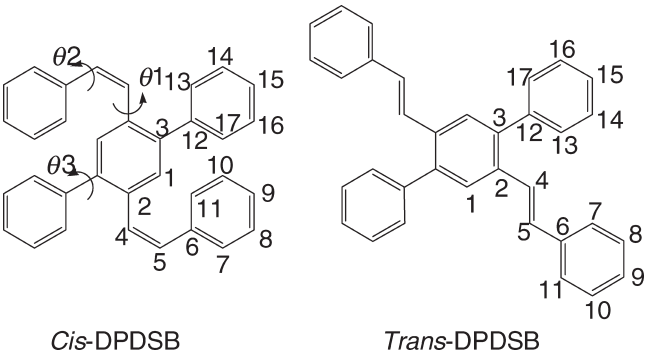

Scheme 2. Structures of *cis*- and *trans*-DPDSB

the decreased conjugation in the distyrylbenzene direction in *cis*-DPDSB. Also, unlike in *trans*-DPDSB, the δ values of the other protons [H7(H11), H8(H10) and H13(H17), H14(H16)] in the end phenyl rings in *cis*-DPDSB are all distributed in a small range from 7.27 to 7.35 ppm. In The ^{13}C NMR spectra of *cis*-DPDSB, C9 and C15 are also indistinguishable and the difference in δ between C8(C10) and C14(C16) or C7(C11) and C13(C17) in *cis*-DPDSB are smaller than those in *trans*-DPDSB. All of the above information indicates that the conjugation effect in the distyrylbenzene direction in *trans*-DPDSB is higher than that in *cis*-DPDSB. The lower conjugation effect in *cis*-DPDSB is caused by the torsion conformation.

IR spectroscopy is one of the most important analytical methods for *cis*/*trans*-isomer characterization. It provides fast and easy criteria, albeit empirical, distinguishing between the isomers (Fig. 3). The spectrum of *trans*-DPDSB shows a strong absorption band at 964 cm^{-1} (out-of-plane bending mode of the C—H bond in the *trans*-vinylene group, β),[45] which is completely absent in the spectrum of *cis*-DPDSB. Unlike in *cis*-DPDSB, the two double bands at about 700 and 760 cm^{-1} (five adjacent H on phenyl)[45] in *trans*-DPDSB indicate the difference in the end rings in the distyrylbenzene and

Table 1. ^{1}H and ^{13}C chemical shifts (relative to TMS) of *cis*- and *trans*-DPDSB in DMSO solution

	cis-DPDSB		*trans*-DPDSB	
C or H	^{13}C (ppm)	^{1}H (ppm)	^{13}C (ppm)	^{1}H (ppm)
1	132.1	7.14(s)	128.1	7.81(s)
2	137.5	—	138.0	—
3	135.2	—	134.8	—
4	131.4	6.64(d)	130.6	7.34(d)
5	130.3	6.42(d)	126.9	7.08(d)
6	140.0	—	140.8	—
7(11)	129.5	7.27–7.35	130.5	7.50(d)
8(10)	129.2		129.6	7.33(t)
9	130.3	7.16(t)	128.6	7.24(t)
12	140.5	—	141.0	—
13(17)	128.2	7.27–7.35	127.2	7.39(d)
14(16)	129.0		129.3	7.55(t)
15	129.6	7.16(t)	128.4	7.48(t)

terphenyl directions, which corresponds to the result from NMR analysis.

The IR spectra of *cis*- and *trans*-DPDSB were simulated using the Gaussian98w program package for Windows on a PC. Both geometry optimization and actual frequency calculation were performed with the DFT/B3LYP method at the level of the 6–31G** basis set. The calculated frequencies are corrected by scale factor 0.9613,[46] and agree well with the experimental results. In addition, we use the HyperChem 7.1 software to analyze the vibrational spectra, and all normal modes are identified and confirmed. The absorption band at 783 cm^{-1} in *cis*-DPDSB, which is absent in the *trans*-isomer, is due to the wagging vibration of the C—H bond in *cis*-vinylene groups. Previously, Fan *et al.* assigned an absorption band at about 875 cm^{-1} to the characteristic absorption of *cis*-vinylene groups.[47] However, we note that this absorption band (875 cm^{-1}) appears in the spectra of both *cis*- and *trans*-DPDSB without a distinct difference in intensity. Hence this 875 cm^{-1} band cannot be used to indicate the conformation of *cis*-vinylene groups at least in the DPDSB system. In fact, this band is probably due to the β vibration of single hydrogen (H1) connected to the central phenyl ring.[45]

The single crystal (block crystal) of *cis*-DPDSB is easily obtained in alcohol, whereas just a mix crystal can be obtained from *trans*-DPDSB (for details, see wide-angle x-ray diffraction and DSC discussions). The structure of *cis*-DPDSB in a single crystal is shown in Fig. 4(left) and the crystal data and refinement parameters are given in Table 2. A noteworthy feature of the *cis*-DPDSB crystal is its torsion conformation, which is similar to that obtained from geometry optimization for the *cis*-DPDSB molecule in the gas phase. The torsion angles between the double bond and two adjacent phenyl rings are 43.1° (θ_1) and 38.3° (θ_2). The torsion angle between the central phenyl ring and the adjacent phenyl ring (in the *p*-terphenyl direction) is 52.4° (θ_3), which is larger than that in *p*-terphenyl (38.4°).[48] Also, it must be noted that

Table 2. Crystal data and refinement parameters for *cis*-DPDSB[a]

Crystal parameter	Value
Chemical formula	$C_{34}H_{26}$
Formula weight	434.55
Crystal system	Monoclinic
Space group	$P2_1/c$
Z	2
a (Å)	10.078(4)
b (Å)	13.220(10)
c (Å)	9.756(8)
α (°)	90
β (°)	111.36(3)
γ (°)	90
V (Å^3)	1210.6(14)
ρ_{calc} (g cm^{-3})	1.192
Crystal dimensions (mm)	$0.31 \times 0.26 \times 0.24$
T (°C)	20(2)
2θ range: min., max. (°)	5.32, 50.42
No. of data collected	3110
No. of unique data	1956
No. of data with $F_o \geq 4.0\sigma(F_o)$	623
μ (mm^{-1})	0.067
$R1(F)$, $wR_2(F^2)$, $(I > 2\sigma(I))$	0.0533, 0.0642
$R1(F)$, $wR_2(F^2)$, all data	0.1904, 0.0860
Goodness-of-fit on F^2	0.782

[a] CCDC-226016 contains supplementary crystallographic data for this paper. These data can be obtained free of charge via www.ccdc.cam.ac.uk/conts/retrieving.html [or from the Cambridge Crystallographic Data Centre, 12 Union Road, Cambridge CB21EZ, UK; fax: (+44) 1223 336033; or by e-mail: deposit@ccdc.cam.ac.uk].

all end phenyl rings that connect to the double bond [e.g. ring A shown in Fig. 4(right)] is inserted between the two adjacent rings (shown as rings B and C) of other molecules and the distance between the phenyl ring A and ring B (or ring C) is 3.609 Å, which indicates some intramolecular motions, e.g. twisting of the double bond and twisting of the end phenyl ring that connect to the double bond are not free.

The wide-angle x-ray diffraction patterns of *cis*- and *trans*-DPDSB are shown in Fig. 5. It is noticeable that

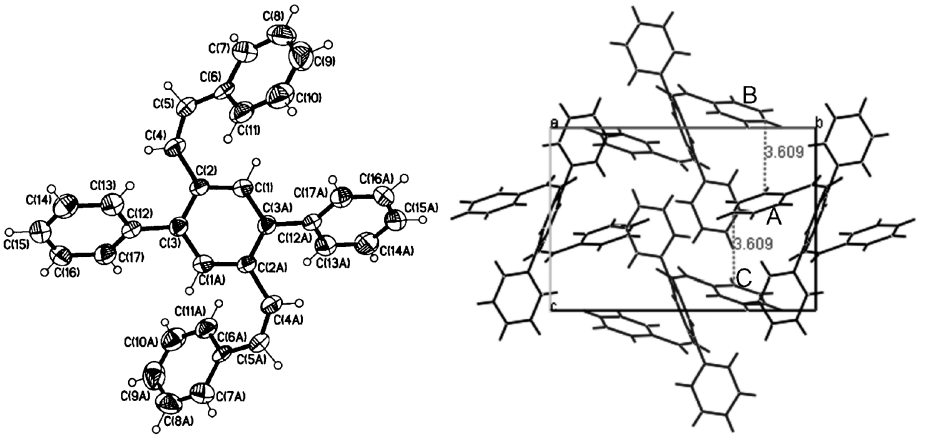

Figure 4. Left: ORTEP drawing of *cis*-DPDSB. The ellipsoid probability is 25%. Right: packing arrangement of *cis*-DPDSB, viewed down the *a*-axis. The phenyl ring A that connects to the double bond is inserted between rings B and C of the two adjacent molecules

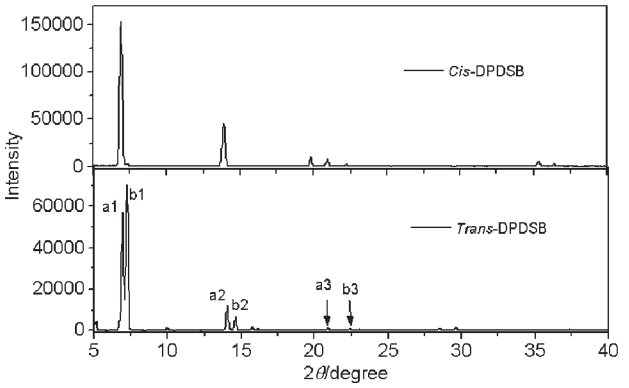

Figure 5. Wide-angle x-ray diffraction patterns of *cis*- and *trans*-DPDSB

several diffractions are very strong in both *cis*- and *trans*-DPDSB crystals. The single peak of the first diffraction at $2\theta = 5.92°$ for *cis*-DPDSB indicates the simplex crystal type, whereas in *trans*-DPDSB the double peak of the first diffraction at $2\theta = 6.96°$ and $7.24°$ (corresponding to interplanar distances of 12.7 and 12.2 Å) is observed (shown as a1 and b1), and a2 and b2 correspond to the second diffraction of the same interplanar distance, etc. These double peaks indicate that the crystals obtained are mixed crystal. As shown in Scheme 3, *trans*-DPDSB is expected to exist as an equilibrium mixture of three rotamers,[49] which may cause different crystal parameters in the crystalline state. We also performed energy optimization by DFT/B3LYP/6–31G of the three rotamers to rationalize their possible existence. The results show that there are three local minima at the three rotamers as expected and the rotamer **a** has the lowest energy. Subsequently, frequency analysis was performed on the optimized structures, and no imaginary frequency was found, which proves that these three rotamers are real stationary points. The existence of mixed crystals of *trans*-DPDSB was further confirmed by DSC experiments. The transformation between the rotamers of *trans*-DPDSB in the crystal is attributed to the invisible but common pedal motion as in stilbene and azobenzene crystals.[50] As for *cis*-DPDSB, such motion may not be occur for the same reason as discussed above and so it cannot transform to other rotamers in the crystal.

Thermal properties of *cis*- and *trans*-DPDSB

The thermal behavior was investigated by means of DSC experiments, using standard heating and cooling rates of $10\,°C\,min^{-1}$ under nitrogen flushing. In the scans shown in Fig. 6, the samples were heated to 210 °C for *cis*-DPDSB and 265 °C for *trans*-DPDSB. The maximum temperatures are obviously below the range of degradation or isomerization according to the coherence of different scan times. Indeed, the resulting samples were examined by FT-IR spectroscopy and no difference was observed before and after the heat treatments, which indicates that there is no isomerization between the two isomers at such temperatures and the difference in the rotamers of *trans*-DPDSB cannot be detected in the FT-IR experiment. For *cis*-DPDSB, the up and down scans in DSC experiments are repeated accurately for the first three times, which indicates high thermal stability. The melting-point of *cis*-DPDSB is 192.5 °C (peak) and no other thermal process is observed, whereas for *trans*-DPDSB there are two peaks in the exotherm of every run shown in Fig. 6 (bottom), which indicates that there may exist two kinds of crystals, as concluded from the wide-angle x-ray diffraction analysis. The change in the relative intensity in the exotherms shows that the proportion of different crystal types altered after the heating process. Also, the endotherm in the second up scan is shifted down by 3 °C and is slightly broader than that in the first up scan. Crystallization is found to occur at peak-to-peak supercooling of 48 and 63 °C for *cis*- and *trans*-isomers, respectively, which are about 10 times larger than *p*-bis(*p*-styrylstyryl)benzene.[51]

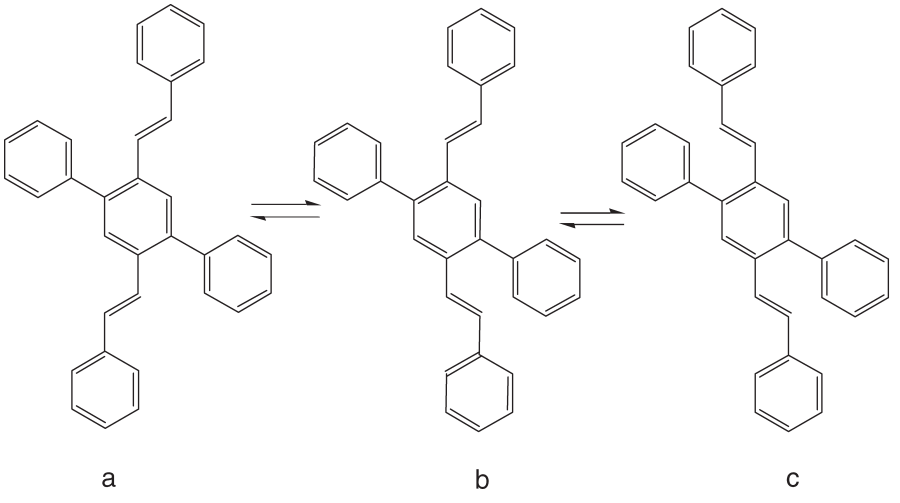

Scheme 3. Equilibrium of three rotamers of *trans*-DPDSB

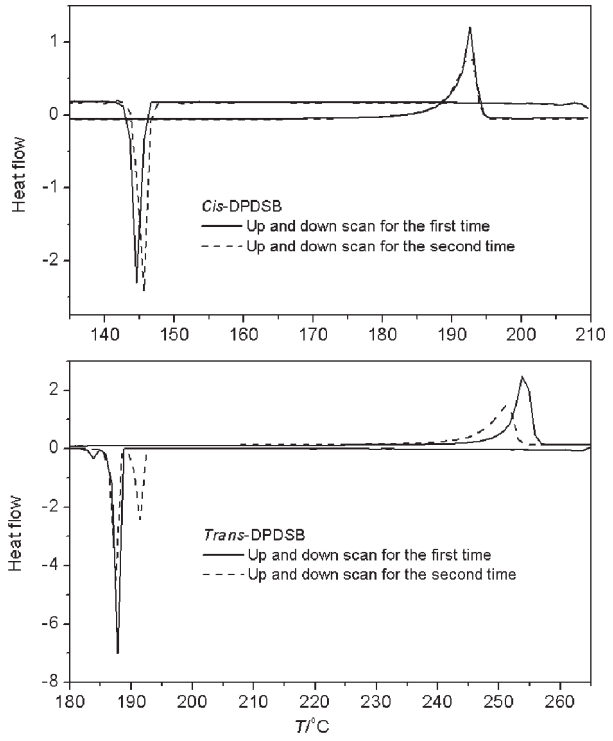

Figure 6. DSC thermograms of *cis*- and *trans*-DPDSB, recorded at heating and cooling rates of 10 °C min^{-1}. Both contain series of first and second heating and cooling processes

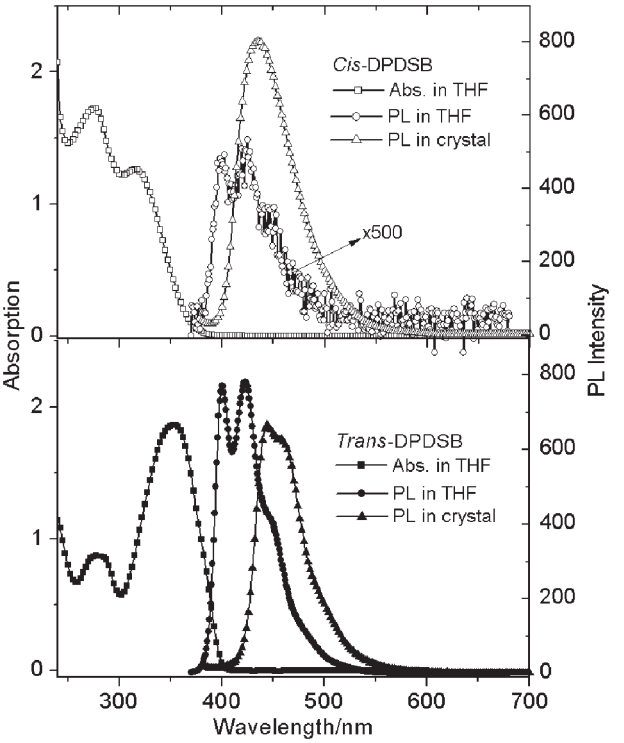

Figure 7. Absorption and emission spectra of the *cis*- and *trans*-DPDSB in dilute THF solution and emission spectra of their crystals. The emission spectra of the *cis*- and *trans*-DPDSB in dilute THF solution were recorded under the same conditions and the spectrum of *cis*-isomer is enlarged 500 times for comparison

Optical properties of *cis*- and *trans*-DPDSB

The absorption and emission spectra of the *cis*- and *trans*-DPDSB in dilute THF solution and the emission spectra of their crystals are shown in Fig. 7 and detailed data are given in Table 3. The absorption spectrum of *cis*-DPDSB in dilute THF solution shows an absorption band at 316 nm with a molar absorption coefficient of 21 900 M^{-1} cm^{-1}, whereas for *trans*-DPDSB the maximum absorption band is at 354 nm with a molar absorption coefficient of 48 500 M^{-1} cm^{-1}. It is the torsion conformation of *cis*-DPDSB that induces a large blue shift in the absorption spectrum and a small molar absorption coefficient. *trans*-DPDSB in dilute THF solution exhibits intense emission as a pure blue band with a high photoluminescence (PL) efficiency of 0.95, whereas the *cis*-DPDSB–THF solution shows almost no fluorescence initially, but after it has been exposed under an ultraviolet lamp (360 nm) for several seconds the fluorescence increases dramatically. Evidently the photochemical processes (*cis–trans* isomerization and photocyclization to 7,14-diphenyldibenzo[*a*,*h*]anthracene) occur and the *trans*-isomer plays the role of the following emission.[52,53] Hence the reason for *cis*-DPDSB showing no fluorescence is that such complicated photochemical processes compete with the luminescence process.[52] Usually the unsubstituted *trans*-OPVs (oligomeric phenylenvinylene) show weak fluorescence in the solid due to 'herringbone'-type crystal packing and strong π–π interaction.[51,54] The crystals of both *cis*- and *trans*-DPDSB show strong fluorescence with maximum emission bands at 435 and 444 nm, respectively (see Figs 7 and 8), which is probably attributable to the weak intermolecular interaction existing in both isomers owing to the large steric hindrance induced by the substituted phenyl groups. Especially for *cis*-DPDSB the photochemical processes that exist in solution are limited by the crystal lattice (see the crystal analysis), that is, the energy barrier from the *cis*-isomer to

Table 3. Optical properties of *cis*- and *trans*-DPDSB

Material	λ_a in solution (nm)	ε ($\times 10^3$) (M^{-1} cm^{-1})	λ_f[a] in solution (nm)	λ_f[b] in crystal (nm)	ϕ_{PL}[c] (solution)
cis-DPDSB	276, 316	21.9 ($\lambda = 316$ nm)	—	435	<0.05
trans-DPDSB	282, 354	48.5 ($\lambda = 354$ nm)	400, 423	444	0.95

[a] Emission spectra were recorded in dilute THF solutions, excited at 350 nm.
[b] In crystals, excited at 360 nm.
[c] In dilute THF, using quinine sulfate in 0.1 M sulfuric acid as standard.

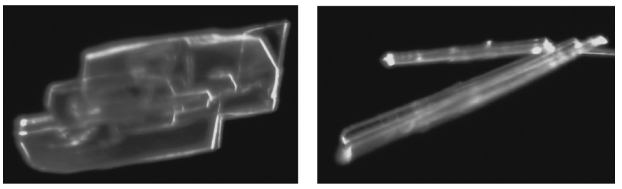

Figure 8. Crystals of *cis*-DPDSB (left, block crystal) and *trans*-DPDSB (right, acicular crystal) under an ultraviolet lamp (365 nm)

the *trans*-isomer/7,14-diphenyldibenzo[*a*,*h*]anthracene is increased dramatically so that the photochemical processes become impossible. Hence the excited state cannot be decayed by isomerization or photocyclization and then the emission process occurs.[52,53] The property of strong emission in the solid state is rare but useful in devices, because the organics are normally used in the solid state.[55]

Electrochemical properties

We investigated the electrochemical behavior of *cis*- and *trans*-DPDSB by cyclic voltammetry (CV). Through the CV curve shown in Fig. 9, three redox steps are observed, of which two appear in the reductive potential range (1,4-distyrylbenzene also shows two reversible waves at -2.48 and -2.74 V in THF)[56] and one in the oxidative potential range. The detailed data are given in Table 4. The reduction waves of *cis*-DPDSB are at -2.30 and -2.52 V and the quasi-reversible anodic wave is at 0.94 V. In contrast, the two reduction waves of *trans*-DPDSB are shifted to -2.21 and -2.51 V and the oxidation wave is at 0.88 V. Therefore, the bandgaps (the energy difference between the HOMO and the LUMO, or between the first oxidation and the first reduction potential) of *cis*- and *trans*-DPDSB can be calculated as 3.16 and 2.97 eV, respectively, which are close to the data obtained from absorption spectra. The decrease of the bandgap caused by changing *cis*- to *trans*-DPDSB can be explained by a stronger torsion within the molecule in the case of the *cis* compared with the *trans* configuration.[57] Because of the steric hindrance, the outer phenyl rings in the distyrylbenzene direction are distorted against the central phenylene unit, which leads to a shorter conjugation length and a larger HOMO–LUMO distance.

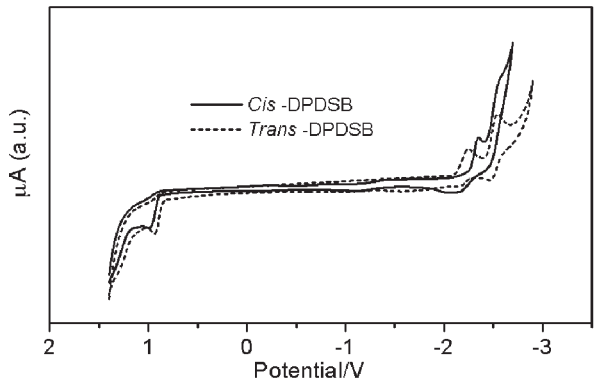

Figure 9. Cyclic voltammograms of *cis*- and *trans*-DPDSB

Frontier molecular orbitals

The frontier orbitals of *cis*- and *trans*-DPDSB were investigated (B3LYP/6–31G), as shown in Fig. 10. For both isomers, the HOMO and LUMO are completely localized on the distyrylbenzene and the node distribution is similar to that in 1,4-distyrylbenzene.[56] Obviously, the LUMO has more nodes than the HOMO in the central benzene rings. In the HOMO the π-bond between C4 and C5 is bonding, whereas the π-bond between C2 and C4 is antibonding. In contrast, in the LUMO the π-bond between C2 and C4 is bonding, whereas the π-bond between C4 and C5 is antibonding. For *cis*-DPDSB, both the HOMO-1 and LUMO + 1 are localized on the terphenyl part, but in *trans*-DPDSB, the HOMO-1 localized on distyrylbenzene, which may be caused by the planar configuration. Hence we can readily conclude that the contribution to fluorescence is due to distyrylbenzene, not terphenyl, whether it is in *cis*- or *trans*-DPDSB.

Cation radical and anion radical properties

To reveal the effects of charge injection on the molecular conformational stability, we calculated structural and electronic properties of both the anion radical and the cation radical. For this purpose, geometry optimization was carried out on both molecular ions (i.e. the neutral molecule in the presence of an extra electron and that of an extra hole, respectively). The optimized structures for both the cation radical and the anion radical show dramatic structural changes relative to the neutral molecule. The distribution of the extra hole in the cation radical calculated as excess spin densities (Fig. 11) is completely localized on the distyrylbenzene and is especially similar to the HOMO and LUMO of the neutral molecule. A similar result is found in the anion radical, where the distribution of the electron is also all localized on the distyrylbenzene. These results indicate that the distyrylbenzene has more sensitive electroactivity than the terphenyl.

The main structural distortions in both the cation radical and the anion radical relative to the neutral molecule are given in Table 5. It is found that the variation of bond lengths and torsion angles in the distyrylbenzene are strongly affected by charge injection, whereas few change takes place in the terphenyl. Moreover, adding a hole has nearly the same effect on structural geometries as adding an electron, and *cis*- and *trans*-DPDSB have the same variation tendency for different charge injections. The C2—C4 bond lengths are shortened by about 0.03 Å and C5—C6 by about 0.02 Å.

Table 4. Redox potentials determined by cyclic voltammetry and the HOMO–LUMO distances determined by electrochemical (measured in DMF) and optical experiments (measured in THF)

Material	$E_{1/2}$(Ox)[a] (V)	$E_{1/2}$(Red1) (V)	$E_{1/2}$(Red2) (V)	$E^{ox}{}_{onset}$[b] (V)	$E_{onset}{}^{red}$ (V)	E^{el} g[c] (eV)	E^{opt} g[d] (eV)
cis-DPDSB	0.94	−2.30	−2.52	0.90	−2.26	3.16	3.36
trans-DPDSB	0.88	−2.21	−2.51	0.84	−2.13	2.97	3.10

[a] $E_{1/2} = (E_{pa} + E_{pc})/2$.
[b] E_{onset} = redox and reductive potential onset.
[c] E^{el}g = band gap from electrochemistry.
[d] E^{opt}g = band gap from UV–visible absorption spectrum (obtained from the edge).

In contrast, the vinylene C═C bonds are lengthened by about 0.02 Å; however, the anion radical has a larger change than the cation radical. In the central phenyl ring, the C1—C2 and C2—C3 bond lengths increase by about 0.01 and 0.02 Å, respectively, and the C1—C3 bond length decreases by about 0.01 Å. In the distyrylbenzene, the torsion angles between the phenyl ring and vinylene double bond are evidently reduced by the positive charge or negative charge, and the maximum variation is more than 14° in the torsion angles between the central phenyl ring and vinylene double bond. In contrast, the torsion angles with respect to the vinylene double bond are increased to different extents, about 9° for *cis*-DPDSB, and <1° for *trans*-DPDSB. Based on the structural changes for both the cation radical and the anion radical discussed above, increased conjugation occurs on the distyrylbenzene, and it is evident that the distyrylbenzene appears to be more coplanar in *trans*-DPDSB than in *cis*-DPDSB. In addition, relative structural stability versus the injection of one charge will be expected for *cis*- and *trans*-DPDSB molecules.

Additional information derived from our calculations provides insight into the interrelationship of structure and electronic behavior, in particular the response of the molecule to the formation of a hole or the addition of an electron. Table 6 contains the results for ionization potentials (*IP*s), electron affinities (*EA*s), both vertical (v: for the geometry of the neutral molecule) and adiabatic

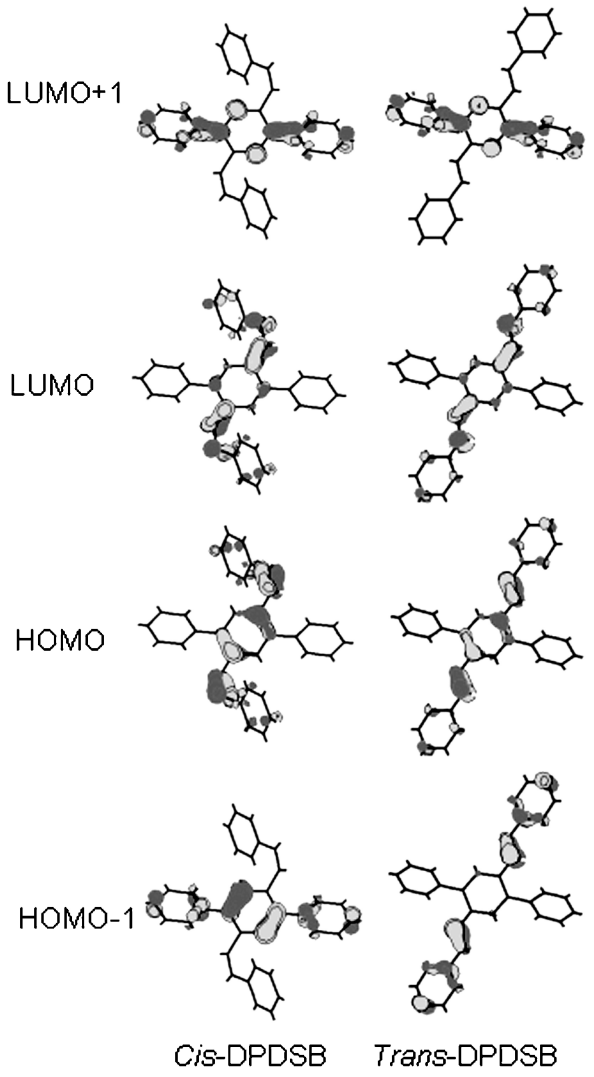

Figure 10. Frontier molecular orbitals of *cis*- and *trans*-DPDSB

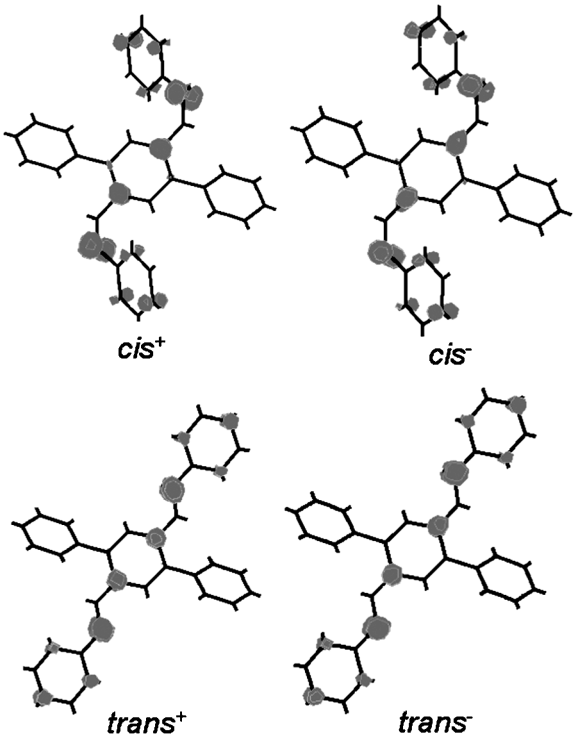

Figure 11. Spin density surfaces of the cation radical and the anion radical for *cis*- and *trans*-DPDSB

Table 5. Main structural parameters of the cation radical and anion radical of *cis*- and *trans*-DPDSB relative to the neutral molecules[a]

	cis-DPDSB		*trans*-DPDSB	
Parameter	Cation	Anion	Cation	Anion
C1—C2	0.014	0.017	0.0224	0.0264
C2—C3	0.0235	0.0248	0.0233	0.0225
C1—C3#	−0.0129	−0.0106	−0.0222	−0.0188
C2—C4	−0.0332	−0.0354	−0.0332	−0.0334
C4—C5	0.024	0.0283	0.0239	0.0273
C5—C6	−0.0238	−0.0216	−0.0235	−0.021
C3—C12	−0.0059	−0.0009	−0.0033	−0.001
C1—C2—C4—C5	−12.64	−14.53	−14.67	−14.83
C2—C4—C5—C6	9.33	8.86	0.6	0.07
C4—C5—C6—C11	−6.99	−12.72	−4.6	−3.96
C2—C3—C12—C13	−0.83	−2.86	4.12	0.13

[a] The numbers of the C atoms correspond to those in Scheme 2. Bond lengths are reported in Å and torsion angles in degrees.

(a: optimized structure for both the neutral and charged molecule) and extraction potentials (*HEP* and *EEP* for the hole and electron, respectively) that refer to the geometry of the ions.[58] *IP*(v) and *IP*(a) of *cis*-DPDSB are larger about 0.2 eV than that of *trans*-DPDSB, and the absolute of value of *EA*(v) and *EA*(a) for *cis*-DPDSB are lower by about 0.28 and 0.15 eV than those for *trans*-DPDSB, respectively. This indicates that the *trans*-isomer can more easily gain or lose an electron, which is in agreement with their energy of the HOMO and LUMO.

Electroluminescence (EL) properties

To investigate the EL properties of *cis*- and *trans*-DPDSB, we fabricated multilayer organic light-emitting devices (OLEDs) with the structure ITO–NPB (50 nm)–*cis*- or *trans*-DPDSB (30 nm)–BCP (10 nm)–Alq_3 (10 nm)–LiF (0.5 nm)–Al, where NPB (*N*,*N*′-di-1-naphthyl-*N*,*N*′-diphenylbenzidine) acts as a hole-transporting layer, *cis*- or *trans*-DPDSB as an emitting layer, BCP (bathocuproin) as an exciton-blocking layer and Alq_3 [tris(8-hydroxyquinolinato)aluminum] as an electron-transporting layer. The normalized EL spectra of devices with various materials are shown in Fig. 12 (left). It can be seen that the EL spectral features of both devices appear in the blue emission region with peaks at 440 and 464 nm for *cis*- and *trans*-DPDSB with CIEs (Commission Internationale de l'Eclairage) of 0.1839, 0.1757 and 0.1797, 0.2189, respectively. As shown in Fig. 12 (right), peak luminances of 1094 and 1643 cd m^{-2} are achieved at

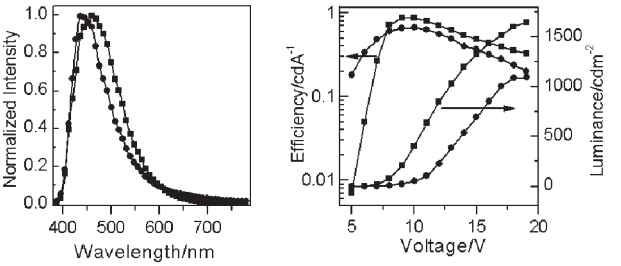

Figure 12. Left: EL spectra of OLEDs of *cis*- (circles) and *trans*-DPDSB (squares), obtained when the voltage is 15 V. Right: luminance and efficiency versus voltage of the OLEDs

a voltage of 19 V, and efficiencies of 0.66 and 0.87 cd A^{-1} are achieved at voltage of 10 V for *cis*- and *trans*-DPDSB, respectively. Obviously, although relatively lower luminance and efficiency are obtained in the device using *cis*-DPDSB, the EL has a more excellent pure blue emission.

CONCLUSION

cis- and *trans*-DPDSB were synthesized and characterized by various spectroscopic and electrochemical methods, including NMR spectroscopy, FT-IR spectroscopy, x-ray crystallography and absorption and electrochemical measurements. These physicochemical data were analyzed together with the results of molecular orbital calculations. The synthetic procedure was carefully optimized, allowing the unusual *cis*-DPDSB to be obtained directly. The main results are summarized as follows. (1) Syntheses of *cis*- and *trans*-DPDSB are achieved by the Wittig reaction by using benzyltriphenylphosphonium bromide and 1,1′;4′,1″-terphenyl-2′,5′-dicarbaldehyde in a 2.2:1 molar ratio at room temperature, and the yields are relatively high. Compared with other methods, such as HPLC, controlling synthetic conditions becomes a more straightforward route to obtain *cis*-isomers. (2) The ^{1}H NMR and IR spectra of the new compounds are entirely consistent with the expected molecular structures: *cis*- and *trans*-DPDSB give clear NMR characteristic signals for the double bonds, and *trans*-DPDSB shows the characteristic IR absorption band of the *trans*-vinylene groups, which is absent completely in *cis*-DPDSB. (3) The x-ray crystal structure of *cis*-DPDSB indicates a deviation from planarity in the distyrylbenzene direction, whereas *trans*-DPDSB tends to form mixed crystals as revealed by wide-angle x-ray diffraction and DSC experiments. (4) Both *cis*- and *trans*-DPDSB have relatively high melting-points and excellent

Table 6. Ionization potentials and electron affinities of *cis*- and *trans*-DPDSB

Material	*IP*(v) (eV)	*IP*(a) (eV)	*HEP* (eV)	*EA*(v) (eV)	*EA*(a) (eV)	*EEP* (eV)	*SPE*(h) (eV)	*SPE*(e) (eV)
cis-DPDSB	6.5930	6.4155	−6.2341	−0.2633	−0.5701	0.7988	0.1775	0.3068
trans-DPDSB	6.3707	6.2115	−6.0602	−0.5483	−0.7257	0.8934	0.1592	0.1774

thermal stability, making it possible to obtain stable devices using these materials. (5) The *cis*-isomer has a large blue shift in the absorption spectrum and a smaller molar absorption coefficient in comparison with *trans*-DPDSB, which is due to its torsion conformation and lower conjugation length. Interestingly, although *cis*-DPDSB shows very weak fluorescence in solution, strong blue fluorescence in the crystal is observed owing to limited photochemical processes in the crystal lattice. (6) The HOMO and LUMO are both completely localized on the distyrylbenzene whether it is in *cis*- or *trans*-DPDSB, indicating that it is the distyrylbenzene, not the terphenyl, that contributes to fluorescence in both isomers. A similar result is found in the cation radical or anion radical, where the distribution of the electron is also all localized on the distyrylbenzene. These results indicate that the distyrylbenzene has more sensitive electroactivity than the terphenyl. (7) In OLEDs using these two materials, *trans*-DPDSB has a higher blue luminance and efficiency but *cis*-DPDSB has more excellent pure blue emission.

EXPERIMENTAL

Materials

p-Xylene, phenylboronic acid, *t*-BuOK, bromomethylbenzene, triphenylphosphine and tetrakis(triphenylphosphine) palladium(0) were purchased from Aldrich and used without further purification unless noted otherwise. THF was dried and purified by fractional distillation over sodium–benzophenone and DMF was vacuum distilled over P_2O_5. Column chromatography was performed using silica gel (200–300 mesh).

General experiments

The NMR spectra were recorded on AVANCZ 500 spectrometers at 298 K by utilizing $CDCl_3$ or DMSO-d_6 as solvent and tetramethylsilane (TMS) as standard. The compounds were characterized with a Flash EA 1112, CHNS-O elemental analysis instrument. Single-crystal structural analysis was performed on a Siemens SMART CCD diffractometer with graphite-monochromated Mo Kα radiation ($\lambda = 0.71073$ Å). GC–mass spectra were measured with a Finnigan TRACE MS instrument. IR spectra were recorded on Perkin-Elmer spectrophotometer in the 400–4000 cm^{-1} region using a powder sample on a KBr plate. UV–visible absorption spectra were recorded on a UV-3100 spectrophotometer. Fluorescence measurements were carried out with an RF-5301PC instrument. The mixed crystal was detected with a Rigaku x-ray diffractometer (*D*/max *r A*, using Cu Kα radiation of wavelength 1.542 Å). Differential scanning calorimetric (DSC) measurements were performed on a Netzsch DSC-204 instrument at heating and cooling rates of 10 °C min^{-1} under nitrogen flushing.

Electrochemical measurements were performed with a BAS 100 W instrument (Bioanalytical Systems) using a platinum disk ($\Phi = 2.0$ mm) as working electrode, platinum wire as auxiliary electrode, with a porous ceramic wick, and Ag/Ag^+ as reference electrode, standardized for the redox couple ferricinium/ferrocene ($E_{1/2} = +0.40$ V, $\Delta E_P = 76$ mV). Cyclic voltammetric studies of the *cis*- and *trans*-DPDSB were carried out at a scan rate of 50 mV s^{-1} on 0.01 M solutions in DMF containing 0.1 M Bu_4NBF_4 as supporting electrolyte. All solutions were purged with a nitrogen stream for 10 min before measurement. The procedure was performed at room temperature and a nitrogen atmosphere was maintained over the solution during measurements.

Theoretical method

The ground-state geometries of different conformations were fully optimized using the density functional theory (DFT), B3LYP/6–31G, as implemented in Gaussian 98. ZINDO and TD-DFT/B3LYP calculations of the vertical excitation energies were then performed at the optimized geometries of the ground states. The excited geometries were optimized by *ab initio* CIS/3–21G. All of I_ps and E_as in this paper are the difference energies between the ions and molecules.

Fabrication of electroluminescent devices

The configuration of devices with multi-layers was optimized for *cis*- and *trans*-DPDSB. Organic layers were deposited by high-vacuum [10^{-6} Torr (1 Torr = 133.3 pa)] thermal evaporation on to a cleaned glass substrate precoated with transparent, conductive indium tin oxide (ITO). The layer thickness of the deposited material was monitored *in situ* using an oscillating quartz thickness monitor. Finally, an LiF buffer layer and an Al cathode were vapor-deposited at a background pressure of 10^{-6} Torr on to the organic films. EL spectra and CIE coordination of these devices were measured with a Spectroscan PR650 spectrometer. The luminance–current density–voltage characteristics were recorded simultaneously with the measurement of the EL spectra by combining the spectrometer with a Keithley Model 2400 programmable voltage–current source. All measurements were carried out at room temperature under ambient conditions.

Syntheses

*1,4-Dibromo-2,5-dimethylbenzene (***1***).*[59] Bromine (65.5 g, 0.41 mol, 2.05 equiv.) was added dropwise, over 30 min,

to a stirred and ice-cooled solution of *p*-xylene (0.2 mol) and iodine (0.2 g, 1.6 mmol), with rigorous exclusion of light. After 1 day at room temperature, 20% KOH solution (50 ml) was added and the mixture was cooled to room temperature, the aqueous solution was decanted and the remaining residue was recrystallized from EtOH (2×200 ml) (34 g, yield 64.4%), m.p. 72–75 °C. ^{1}H NMR (500 MHz, 25 °C, $CDCl_3$, TMS, ppm), δ 7.39 (s, 2H; benzo H), 2.33 (s, 6H; CH_3); FT-IR (KBr pellet, cm^{-1}), 2978(m), 2952(m), 2916(w), 2848(w), 1749(m), 1473(s), 1433(s), 1375(m), 1342(m), 1293(w), 1186 (m), 1055(s), 982(s), 879(s), 748(s).

2,5-Dibromobenzene-1,4-dicarbaldehyde (**2**). This compound was synthesized according to a published procedure with minor modification.[60] Sulfuric acid (28 ml) was added dropwise to a suspension containing **1** (8.0 g), acetic acid (40 ml) and acetic anhydride (80 ml) at 0 °C. CrO_3 (12 g) was then added to the mixture in portions. The resulting mixture was stirred vigorously at this temperature for a further 5 h until the reaction was completed. The greenish slurry was poured into ice–water and filtered. The white solid was washed with water and cold methanol. The diacetate was then hydrolyzed by refluxing with a mixture of water (40 ml), ethanol (40 ml) and sulfuric acid (4 ml) for 5 h. After the mixture had cooled, the pale yellow product was separated by filtration. The crude product was purified by recrystallization from chloroform (4.3 g, yield 48.6%), m.p. 194 °C. ^{1}H NMR (500 MHz, 25 °C, $CDCl_3$, TMS, ppm), $\delta = 10.35$ (s, 2H; CHO), 8.16 (s, 2H; benzo H); FT-IR (KBr pellet, cm^{-1}), 3074(m), 2873(m), 1687(vs), 1444(m), 1342(s), 1276(m), 1157(m), 1057(s), 914(m), 812(m).

1,1′;4′,1-Terphenyl-2′,5′-dicarbaldehyde (**3**). This compound was synthesized by the well-known Suzuki coupling method.[61] A mixture of **2** (1.0 g), phenylboronic acid (1.1 g), $Pd(PPh_3)_4$ (0.2 g), toluene (12.5 ml) and 2 M Na_2CO_3 solution (2.5 ml) was refluxed at 85 °C for 36 h under nitrogen, then poured into water and extracted with dichloromethane. The organic layer was washed with brine and water and dried over $MgSO_4$. The crude product was first purified by flash column chromatography (dichloromethane as eluent) and then recrystallized form chloroform. A 0.79 g amount of product (yield 81%) was obtained as pale yellow crystals, m.p. 197–200 °C. ^{1}H NMR (500 MHz, 25 °C, $CDCl_3$, TMS, ppm), δ 10.09 (s, 2H; CHO), 8.12 (s, 2H; benzo H), 7.53–7.44 (m, 10H; benzo H); FT-IR (KBr pellet, cm^{-1}), 3024(w), 2889(w), 1678(vs), 1469(m), 1446(m), 1390(m), 1267(w), 1242 (w), 1149(m), 1076(w), 1022(w), 904(w), 837(s), 766 (m), 706(s).

Benzyltriphenylphosphonium bromide. This compound was synthesized with a molar ratio of 1:1.05 of (bromomethyl)benzene and triphenylphosphine. Bromomethylbenzene (2.565 g) was dropped into DMF solution containing triphenylphosphine (4.12 g) and refluxed for 12 h. The resulting solution was evaporated under decreased pressure and the crude product was washed with cyclohexane (50 ml) and recrystallized from dichloromethane (100 ml). The white precipitates were collected via filtration and dried under vacuum (5.65 g, yield 87%), m.p. 294–295 °C. ^{1}H NMR (500 MHz, 25 °C, $CDCl_3$, TMS, ppm), δ 7.8–7.7 (m, 9H; benzo H), 7.64 (t, 6H; benzo H), 7.23 (t, 1H; benzo H), 7.14 (t, 2H; benzo H), 7.09 (d, 2H; benzo H), 5.42 (d, 2H; CH_2); FT-IR (KBr pellet, cm^{-1}), 3049(m), 2985(m), 2850(m), 2777(m), 1585(m), 1495(m), 1437(s), 1161(m), 1111(s), 995(m), 875(m), 790(m), 756(s), 719(s), 690(s).

2,5-Diphenyl-1,4-distyrylbenzene with two *cis* double bonds (*cis*-DPDSB). The phosphonium salt (200 mg) and **3** (660 mg) were placed in a dry flask, which was wrapped with tinfoil, and the flask was flushed with nitrogen. Dry, cooled THF (30 ml) was added to the flask via an injector and then *t*-BuOK in dry THF was added slowly to allow the colored ylide formed to react with aldehyde groups between successive additions. When no color was observed upon addition of base, the mixture was stirred for a further 12 h at room temperature. After the reaction was completed, most of the solvent was removed under reduced pressure and then the concentrated solution was dropped into stirred methanol (50 ml). A 255 mg amount of white product was obtained by filtration (yield 87%), m.p. 192.5 °C. ^{1}H NMR (500 MHz, 25 °C, DMSO, TMS, ppm), δ 7.27–7.35 (m, 16H; benzo H), 7.16 [t, J(HH) = 1.5 Hz, 4H; benzo H], 7.14 (s, 2H; benzo H), 6.64 [d, J(HH) = 12 Hz, 2H; olefinic H] 6.42 [d, J(HH) = 12 Hz, 2H; olefinic H]; ^{13}C NMR (500 MHz, 25 °C, DMSO, TMS, ppm), δ 140.5, 140.0, 137.5, 135.2, 132.1, 131.4, 130.3, 129.6, 129.5, 129.2, 129.0, 128.2; FT-IR (KBr pellet, cm^{-1}), 3056(m), 1599(w), 1493(w), 1475(m), 1444(m), 1408(w), 1385(w), 1074(m), 1026(m), 870(vw), 783(s), 764(s), 698(vs); MS: *m/z* 434.2 (M). Anal. calcd for $C_{34}H_{26}$, C 93.97, H 6.03; found, C 93.83, H 6.17%.

2,5-Diphenyl-1,4-distyrylbenzene with two *trans* double bonds (*trans*-DPDSB). This material was prepared by refluxing a *p*-xylene solution of the *cis*-isomer (200 mg) for 12 h in the presence of a small amount of iodine as catalyst. The resulting solution was concentrated using a rotatory evaporator and then dropped into stirred methanol (20 ml). A 190 mg amount of yellow product was obtained by filtration (yield 95%), m.p. 251–254 °C. ^{1}H NMR (500 MHz, 25 °C, DMSO, TMS, ppm), δ 7.81(s, 2H; benzo H), 7.55 [t, J(HH) = 7.36 Hz, 4H; benzo H], 7.50 [d, J(HH) = 7.22 Hz, 4H; benzo H], 7.48 [t, J(HH) = 7.21 Hz, 2H; benzo H], 7.39 [d, J(HH) = 7.33 Hz, 4H; benzo H], 7.34 [d, J(HH) = 16.31 Hz, 2H; olefinic H], 7.33 [t, J(HH) = 7.49 Hz, 4H; benzo H], 7.24 [t, J(HH) = 7.25 Hz, 2H; benzo H], 7.08 [d, J(HH) = 16.35 Hz, 2H;

olefinic H]; ^{13}C NMR (500 MHz, 25 °C, DMSO, TMS, ppm), δ 141.0, 140.8, 138.0, 134.8, 130.6, 130.5, 129.6, 129.3, 128.6, 128.4, 128.1, 127.2, 126.9; FT-IR (KBr pellet, cm^{-1}), 3053(m), 1595(m), 1493(m), 1477(m), 1446(m), 1396(w), 1340(w), 1072(m), 1024(m), 964(s), 922(w), 901(m), 877(vw), 852(w), 764(vs), 752(s), 704(vs); MS, *m/z* 434.2 (M). Anal. calcd for $C_{34}H_{26}$, C 93.97, H 6.03; found, C 93.85, H 6.15%.

Acknowledgments

We are grateful for financial support from the National Science Foundation of China. (grant numbers 20474024, 20125421, 90101026 and 50303007) and from the Ministry of Science and Technology of China (grant numbers 2002CB6134003 and 2003CB314703).

REFERENCES

1. Clery D. *Science* 1994; **263**: 1700–1702.
2. Kraft A, Grimsdale AC, Holmes AB. *Angew. Chem.* 1998; **110**: 416–443; *Angew. Chem. Int. Ed.* 1998; **37**: 402–428.
3. Burroughes JH, Bradley DDC, Brown AR, Marks RN, Mackay K, Friend RH, Burns PL, Holmes AB. *Nature* 1990; **347**: 539–541.
4. Scherf U, List EJW. *Adv. Mater.* 1998; **14**: 477–487.
5. Braun D, Heeger AJ. *Appl. Phys. Lett.* 1991; **58**: 1982–1984.
6. Shi Y, Liu J, Yang Y. *J. Appl. Phys.* 2000; **87**: 4254–4263.
7. Wan WC, Antoniadis H, Choong VE, Razafitrimo H, Gao Y, Feld WA, Hsieh BR. *Macromolecules* 1997; **30**: 6567–6574.
8. Hsieh BR, Antoniadis H, Bland DC, Feld WA. *Adv. Mater.* 1995; **7**: 36–39.
9. Hsieh BR, Wan WC, Yu Y, Gao Y, Goodwin TE, Gonzalez SA, Feld WA. *Macromolecules* 1998; **31**: 631–636.
10. Greenham NC, Moratti SC, Bradley DDC, Friend RH, Holmes AB. *Nature* 1993; **365**: 628–630.
11. Chen SA, Chang EC. *Macromolecules* 1998; **31**: 4899–4907.
12. Jenekhe SA, Osaheni JA. *Science* 1994; **265**: 765–768.
13. Jakubiak R, Collison CJ, Wan WC, Rothberg LJ, Hsieh BR. *J. Phys. Chem. A* 1999; **103**: 2394–2398.
14. Yan M, Rothberg LJ, Kwock EW, Miller TM. *Phys. Rev. Lett.* 1995; **75**: 1992–1995.
15. Chen SH, Su AC, Han SR, Chen SA, Lee YZ. *Macromolecules* 2004; **37**: 181–186.
16. Vanden Bout DA, Yip WT, Hu D, Fu DK, Swager TM, Barbara PF. *Science* 1997; **277**: 1074–1077.
17. Nguyen TQ, Doan V, Schwartz BJ. *J. Chem. Phys.* 1999; **110**: 4068–4078.
18. Nguyen TQ, Martini IB, Liu J, Schwartz BJ. *J. Phys. Chem. B* 2000; **104**: 237–255.
19. Hsieh BR, Yu Y, Forsythe EW, Schaaf GM, Feld WA. *J. Am. Chem. Soc.* 1998; **120**: 231–232.
20. Peng Z, Zhang J, Xu B. *Macromolecules* 1999; **32**: 5162–5164.
21. Spreitzer H, Becker H, Kluge E, Kreuder W, Schenk H, Demandt R, Schoo H. *Adv. Mater.* 1998; **10**: 1340–1343.
22. Müllen K, Wegner G. *Electronic Materials: The Oligomer Approach*. Wiley-VCH: Weinheim, 1998.
23. Martinez-Ruiz P, Behnisch B, Schweikart KH, Hanack M, Lüer L, Oelkrug D. *Chem. Eur. J.* 2000; **6**: 1294–1301.
24. Liao L, Pang Y, Ding L, Karasz FE. *Macromolecules* 2001; **34**: 7300–7305.
25. Stalmach U, Schollmeyer D, Meier H. *Chem. Mater.* 1999; **11**: 2103–2106.
26. Tian B, Zerbi G, Schenk R, Müllen K. *J. Chem. Phys.* 1991; **95**: 3191–3197.
27. Zojer E, Knupfer M, Shuai Z, Fink J, Brédas JL, Hörhold HH, Grimme J, Scherf U, Benincori T, Leising G. *Phys. Rev. B* 2000; **61**: 16561–16569.
28. Meier H, Gerold J, Kolshorn H, Mühling B. *Chem. Eur. J.* 2004; **10**: 360–370.
29. Syamakumari A, Schenning APHJ, Meijer EW. *Chem. Eur. J.* 2002; **8**: 3353–3361.
30. He F, Cheng G, Zhang HQ, Zheng Y, Xie ZQ, Yang B, Ma YG, Liu SY, Shen JC. *Chem. Commun.* 2003; 2206–2207.
31. Henari FZ, Manaa H, Kretsch KP, Blau WJ, Rost H, Pfeiffer S, Teuschel A, Tillmann H, Hörhold HH. *Chem. Phys. Lett.* 1999; **307**: 163–166.
32. Döttinger SE, Hohloch M, Hohnholz D, Segura JL, Steinhuber E, Hanack M. *Synth. Met.* 1997; **84**: 267–268.
33. Strehmel B, Sarker AM, Malpert JH, Strehmel V, Seifert H, Neckers DC. *J. Am. Chem. Soc.* 1999; **121**: 1226–1236.
34. Barashkov NN, Guerrero DJ, Olivos HJ, Ferraris JP. *Synth. Met.* 1995; **74**: 153–160.
35. Vromen S, Modiano A, Mandelvaum A, Ginsburg D, Hwang B, Schlessinger RH, Cava MP. *Tetrahedron* 1966; **22**(Suppl. 7): 203–211.
36. Wong KF, Skaf MS, Yang CY, Rossky PJ, Bagchi B, Hu D, Yu J, Barbara PF. *J. Phys. Chem. B* 2001; **105**: 6103–6107.
37. Chen YS, Meng HF. *Phys. Rev. B* 2002; **66**: 035202.
38. Summers MA, Kemper PR, Bushnell JE, Robinson MR, Bazan GC, Bowers MT, Buratto SK. *J. Am. Chem. Soc.* 2003; **125**: 5199–5203.
39. Claudio GC, Bittner ER. *J. Chem. Phys.* 2001; **115**: 9585–9593.
40. Son S, Dodabalapur A, Lovinger AJ, Galvin ME. *Science* 1995; **269**: 376–378.
41. Yang NC, Jeong JK, Choi SJ, Rhee TH, Suh DH. *Macromol. Rapid Commun.* 1999; **20**: 586–590.
42. Pang Y, Li J, Hu B, Karasz FE. *Macromolecules* 1999; **32**: 3946–3950.
43. Hwang JJ, Lin RL, Shieh RL, Jwo JJ. *J. Mol. Catal. A: Chem.* 1999; **142**: 125–139.
44. Jacobs S, Eevers W, Verreyt G, Geise HJ. *Synth. Met.* 1993; **61**: 189–193.
45. Nakanishi K. *Infrared Absorption Spectroscopy—Practical*. Holden-Day: San Francisco, 1962; 24, 27.
46. Wong MW. *Chem. Phys. Lett.* 1996; **256**: 391–399.
47. Fan QL, Lu S, Lai YH, Hou XY, Huang W. *Macromolecules* 2003; **36**: 6976–6984.
48. Cacelli I, Prampolini G. *J. Phys. Chem. A* 2003; **107**: 8665–8670.
49. Ito Y, Uozu Y, Dote T, Ueda M, Matsuura T. *J. Am. Chem. Soc.* 1988; **110**: 189–198.
50. Harada J, Ogawa K. *J. Am. Chem. Soc.* 2001; **123**: 10884–10888; *J. Am. Chem. Soc.* 2004; **126**: 3539–3544.
51. van Hutten PF, Wildeman J, Meetsma A, Hadziioannou G. *J. Am. Chem. Soc.* 1999; **121**: 5910–5918.
52. Waldeck DH. *Chem. Rev.* 1991; **91**: 415–436, and references cited therein.
53. Dou Y, Allen RE. *J. Chem. Phys.* 2003; **119**: 10658–10666.
54. Wu CC, DeLong MC, Vardeny ZV, Ferraris JP. *Synth. Met.* 2003; **137**: 939–940.
55. Chen J, Law CCW, Lam JWY, Dong Y, Lo SMF, Williams ID, Zhu DB, Tang BZ. *Chem. Mater.* 2003; **15**: 1535–1546.
56. Renak ML, Bartholomew GP, Wang S, Ricatto PJ, Lachicotte RJ, Bazan GC. *J. Am. Chem. Soc.* 1999; **121**: 7787–7799.
57. Lange FJ, Leuze M, Hanack M. *J. Phys. Org. Chem.* 2001; **14**: 474–480.
58. Curioni A, Boero M, Andreoni W. *Chem. Phys. Lett.* 1998; **294**: 263–271.
59. Rehahn M, Schlüter AD, Feast WJ. *Synthesis* 1988; 386–388.
60. Naylor JR. *J. Chem. Soc.* 1952; 4085–4086.
61. Miyaura N, Suzuki A. *Chem. Rev.* 1995; **95**: 2457–2483.